

# Strong gravitational lensing of a five-dimensional charged, equally rotating black hole with a cosmological constant

Md Sabir Ali,<sup>1,2,3,4,\*</sup> Shagun Kaushal,<sup>5,†</sup> and Yu-Xiao Liu<sup>1,2,3,‡</sup>

<sup>1</sup>*Key Laboratory of Quantum Theory and Applications of Ministry of Education,  
Lanzhou Center for Theoretical Physics, Lanzhou University, Lanzhou 730000, China*

<sup>2</sup>*Key Laboratory of Theoretical Physics of Gansu Province,  
Institute of Theoretical Physics & Research Center of Gravitation,  
Lanzhou University, Lanzhou 730000, China*

<sup>3</sup>*School of Physical Science and Technology,  
Lanzhou University, Lanzhou 730000, China*

<sup>4</sup>*Department of Physics, Mahishadal Raj College, West Bengal 721628, India*

<sup>5</sup>*Department of Physics, Indian Institute of Technology Delhi, Hauz Khas, New Delhi-110016, India*

We study the lensing phenomena of the strong gravity regime of the five-dimensional charged, equally rotating black holes with a cosmological constant, familiarly known as the Cvetič-Lü-Pope black holes. These black holes are characterized by three observable parameters, the mass  $M$ , the charge  $Q$  and the angular momentum  $J$ , in addition to the cosmological constant. We investigate the strong gravitational lensing observables, mainly the photon sphere radius, the minimum impact parameter, the deflection angle, the angular size, and the magnification of the relativistic images. We model the  $M87$  and  $SgrA^*$  for these observables. We also focus on the relativistic time delay effect in the strong field regime of gravity and the impact of the observable on it. The analytical expressions for the observables of the relativistic images with vanishing angular momentum ( $j = 0$ ) are discussed in some detail.

---

\* [alimd.sabir3@gmail.com](mailto:alimd.sabir3@gmail.com)

† [shagun1459@gmail.com](mailto:shagun1459@gmail.com)

‡ [liuyx@lzu.edu.cn](mailto:liuyx@lzu.edu.cn), the corresponding author

## I. INTRODUCTION

The recent year witnessed a flurry of activities regarding the astronomical measures of the general relativistic effects, especially the observation of the black hole shadows, e.g., for the M87 and SgA\*, and the gravitational wave data from the LIGO scientific/Virgo collaborations [1–6]. The data from the Event Horizon Telescope (EHT) regarding the shadows of the black holes confirmed the validity of Einstein’s general relativity (GR) and established it as a firm base for any general relativistic theory of gravity [7–12]. As is known from its definition, gravitational lensing is the deflection of light rays when they pass close to black holes [13–15]. Gravitational lensing is utilized as an important tool in astrophysics; for example, it is used to measure the mass of compact objects. The formation of Einstein’s ring is one of the remarkable observations made during the lensing phenomenon. The ring forms when the bright source (the star), the black hole (the lens), and the observer are aligned in a perfect way. Gravitational lensing has been investigated in detail for a variety of black hole solutions in GR as well as in other theories of gravity. For reviews on both weak and strong gravitational lensings in both equatorial ( $\theta = \pi/2$ ) and non-equatorial ( $\theta \neq \pi/2$ ) planes, we refer our readers to Refs. [16–23] and references therein.

From the strong lensing point of view, the light rays pass close enough to the black hole wind once or several times before leaving that region and reaching the observer. The idea that black holes act as gravitational lenses was first put forward by Darwin [13] and subsequently elaborated in Refs. [24, 25]. The most recent theoretical investigation of strong field gravitational lensing is mainly attributed to the seminal work of Virbhadra and Ellis [26, 27], where they discussed the formation of the ring, its position, and the magnification of relativistic images for the Schwarzschild black hole. Soon after this formulation, more rigorous analytical descriptions of the exact lens equation and the integral expressions for its solution were obtained by Frittelli, Killing, and Newman [14]. A comparison of their results with those given by Virbhadra and Ellis was also presented. Later, Bozza [16–19] and then Tsukamoto [28, 29] proposed a completely new method for the study of strong lensing for a generic spherically symmetric static spacetime. These methods are largely accepted by the scientific community and are still used as applications in the study of strong lensing phenomena. These methods were applied to study the various black hole systems, including solutions in various modified theories of gravity [31–45].

The string theory is a promising candidate for the unified theory, where gravity is unified with other forces of nature. The prediction of the extra dimensions and its relation to the physical observable attracted a lot of attention because it borrowed the signature of the string and hence

made string theory a correct one. The extra dimensions can have imprints in the quasinormal modes of the higher-dimensional black holes [46–58], which are believed to be tested through gravitational wave probes in the near future. The higher-dimensional black holes/black branes in the particle accelerators and in the cosmic rays were studied to get an insight into the extra dimensions. Therefore, gravitational lensing can also be used to probe the extra dimensions. In this direction, the study of strong lensing in higher-dimensional black hole solutions is worth investigating. The search for the extra dimensions was probed through the gravitational lensing of a charged-neutral/charged Kaluza-Klein squashed black hole [59–61], the squashed Kaluza-Klein Gödel black hole for both charged and charged-neutral cases [62, 63], the black hole with extra dimensions and the Kalb-Ramond field [64, 65]. These studies help us to understand the effective length scale on which the extra dimension lies. Motivated by these investigations, in our present paper, we wish to study the strong gravitational lensing of the five-dimensional charged equally rotating black hole in the presence of a negative cosmological constant as given in Ref. [66], when the charged scalar hair has vanishing limit. This black hole solution was originally proposed by Cvetič, Lü and Pope [67], hereby denoted as the CLP black hole. Such a solution is considered as a coupling of the Einstein-Maxwell system that arises as the bosonic sector of the minimal-gauged five-dimensional supergravity theories. As for the special cases, such a solution reduces all the previously known cases. The solution is characterized by the mass, the charge, the angular momentum, and the cosmological constant. We shall see how the charge, the rotation parameter, and other defining parameters affect the size of the horizon, the photon sphere radius, the formation of relativistic images, the deflection angle, and subsequently other physical observables in the strong field lensing of gravity.

The organization of the paper is as follows. In Section II, we briefly discuss the solution of the five-dimensional charged equally rotating black hole solution as given by Cvetič, Lü and Pope. We also investigate the horizon structure and parametric bounds on the charge and rotation parameters. Section III is devoted to discussing the formulation of the deflection angle using Bozza’s method. We discuss the effective potential, the photon sphere radius, the impact parameter, and their connections. We also discuss them in the limiting cases, when  $j = 0$ . Next, we discuss the lensing observable and the formation of the relativistic images of the black hole in Section IV. Here, we model our concerned black holes as SgrA\* and M87\* to show the effect of the parameters. In Section V, we discuss the time delay effect. Finally, in Section VI, we summarize the paper and conclude our results.

## II. THE FIVE-DIMENSIONAL CHARGED EQUALLY ROTATING BLACK HOLE SOLUTION WITH A COSMOLOGICAL CONSTANT

We present a brief review of the action and the constituent spacetime before we move on to the main discussion of the lensing phenomena. The expression for the action is given by a consistent truncation and is written as [66, 68]

$$S = \frac{1}{16\pi G_5} \int d^5x \sqrt{-g} \left( R + 12 - \frac{3}{4} F_{\mu\nu} F^{\mu\nu} - \frac{3}{8} \left( |D_\mu \phi|^2 - \frac{\partial_\mu(\phi\phi^*) \partial^\mu(\phi\phi^*)}{4(4 + \phi\phi^*)} - 4\phi\phi^* \right) + \frac{1}{4\sqrt{-g}} \epsilon^{\alpha\beta\gamma\mu\nu} F_{\alpha\beta} F_{\gamma\mu} A_\nu \right), \quad (1)$$

where

$$D_\mu \phi = \partial_\mu \phi - 2i A_\mu \phi, \quad F_{\mu\nu} = \partial_\mu A_\nu - \partial_\nu A_\mu. \quad (2)$$

The variation of the action Eq. (1) with respect to the metric tensor  $g_{\mu\nu}$  yields the Einstein's field equations [66, 68]

$$R_{\mu\nu} - \frac{1}{2} (R + 12) g_{\mu\nu} = -\frac{3}{2} T_{\mu\nu}^{\text{EM}} + \frac{3}{8} T_{\mu\nu}^\phi. \quad (3)$$

The expressions for the energy-momentum tensor of the electromagnetic field  $T_{\mu\nu}^{\text{EM}}$ , and the scalar field  $T_{\mu\nu}^\phi$  are

$$\begin{aligned} T_{\mu\nu}^{\text{EM}} &= F_\mu^\alpha F_{\nu\alpha} - \frac{1}{2} g_{\mu\nu} F_{\alpha\beta} F^{\alpha\beta}, \\ T_{\mu\nu}^\phi &= \frac{1}{2} \left[ D_\mu \phi (D_\nu \phi)^* + D_\nu \phi (D_\mu \phi)^* - \frac{1}{2} g_{\mu\nu} |D_\alpha \phi|^2 + 2\phi\phi^* g_{\mu\nu} \right. \\ &\quad \left. - \frac{1}{4(4 + \phi\phi^*)} \left( \partial_\mu(\phi\phi^*) \partial_\nu(\phi\phi^*) - \frac{1}{2} g_{\mu\nu} [(\partial_\sigma \phi\phi^*) (\partial^\sigma \phi\phi^*)] \right) \right]. \end{aligned} \quad (4)$$

The Maxwell and the scalar field equations are given, respectively, as [66, 68]

$$\nabla_\nu F_\mu^\nu = \frac{i}{4} \left[ \phi (D_\mu \phi)^* - \phi^* (D_\mu \phi) + \frac{1}{4\sqrt{-g}} g_{\mu\sigma} \epsilon^{\sigma\alpha\beta\gamma\nu} F_{\alpha\beta} F_{\gamma\nu} \right], \quad (5)$$

$$D_\mu D^\mu \phi + \left[ \frac{[\partial_\sigma(\phi\phi^*)]^2}{4(4 + \phi\phi^*)^2} - \frac{\nabla^2(\phi\phi^*)}{2(4 + \phi\phi^*)} \right] \phi = 0. \quad (6)$$

The stationary, asymptotically anti-de Sitter spacetimes have spherical horizon topology. The generic solutions to such a structure have two independent rotation parameters. To keep the structure simpler we consider the doubly rotating black hole solutions, having the same magnitude of the rotation parameters but with two different orientations. For any generic gauge choice, we can write down the metric *ansatz* as follows [66]:

$$ds^2 = -f(r) dt^2 + g(r) dr^2 + \Sigma^2(r) \left[ h(r) (d\psi + \frac{1}{2} \cos \theta d\phi - \Omega(r) dt)^2 + \frac{1}{4} d\Omega_2^2 \right], \quad (7)$$

which is rewritten as

$$\begin{aligned}
ds^2 = & \left( -f(r) + \Sigma^2(r)\Omega^2(r)h(r) \right) dt^2 + g(r)dr^2 + \frac{1}{4}\Sigma^2(r)d\theta^2 - \Sigma^2(r)\Omega(r)h(r)\cos\theta d\phi dt \\
& + \frac{\Sigma^2(r)}{4} \left( h(r)\cos^2\theta + \sin^2\theta \right) d\phi^2 + \Sigma^2(r)h(r)d\psi^2 - 2\Sigma^2(r)\Omega(r)h(r)d\psi dt \\
& + \Sigma^2(r)h(r)\cos\theta d\psi d\phi.
\end{aligned} \tag{8}$$

In the above *ansatz*, we can see that the metric on  $S^3$  is expressed as a Hopf fibration over the space  $\mathbb{CP}^1$  of unit radius. In this way, the coordinate  $\psi$  has the period of  $2\pi$  and the  $\theta, \phi$  coordinates have the coordinate ranges of the usual unit  $S^2$  sphere. General five-dimensional, charged, and equally rotating black hole solutions with a cosmological constant were first presented in Ref. [67], which is basically a coupled Einstein-Maxwell solution in the bosonic sector of minimal gauged supergravity, and also  $\phi = 0$  limit of the action (1). The black holes are governed by three hairs  $\{q, j, m\}$ , and an additional fourth parameter, the cosmological constant term. The parameters  $\{q, j, m\}$  are related to the conserved charges  $\{Q, J, M\}$ . The functions appear in the metric (8) have the explicit forms

$$\begin{aligned}
\Sigma(r) &= r, \quad f(r) = \frac{G(r)}{h(r)}, \quad g(r) = \frac{1}{G(r)}, \\
h(r) &= 1 + j^2 \left( \frac{m}{r^4} - \frac{q^2}{r^6} \right), \quad \Omega(r) = \frac{j}{h(r)} \left( \frac{m-q}{r^4} - \frac{q^2}{r^6} \right), \\
G(r) &= \frac{1}{r^4} \left[ q^2 \left( 1 - \frac{j^2}{L^2} \right) + j^2 m \right] - \frac{1}{r^2} \left[ m \left( 1 - \frac{j^2}{L^2} \right) - 2q \right] + \frac{r^2}{L^2} + 1.
\end{aligned} \tag{9}$$

The angular momentum  $J$  and the mass  $M$  of the black hole are related to the parameters  $\{q, j, m\}$  as follows:

$$J = \frac{1}{2}j(m-q), \quad M = \frac{1}{4} \left[ m \left( 3 + \frac{j^2}{L^2} \right) - 6q \right], \quad Q = \frac{q}{2}. \tag{10}$$

Using the last two relations of the above equations we can express  $m$  and  $q$  as

$$m = \frac{2L^2(2M + 6Q)}{j^2 + 3L^2}, \quad q = 2Q. \tag{11}$$

Please note that in the action, we put the AdS radius  $L = 1$ . Here, we restored it for the sake of clarity and calculation. The static and spherically symmetric part of the solution is obtained if one puts

$$ds^2 = -f(r)dt^2 + g(r)dr^2 + \Sigma^2(r)d\Omega_3^2, \tag{12}$$

$$d\Omega_3^2 = (d\psi + \frac{1}{2}\cos\theta d\phi)^2 + \frac{1}{4}d\Omega_2^2 = d\theta^2 + \sin^2\theta d\phi^2 + \cos^2\theta d\psi^2. \tag{13}$$

Obviously, the metric (12) is the five-dimensional Reissner-Nordström black holes with a cosmological constant, where  $f(r)$  and  $g(r)$  are given by [67]

$$f(r) = 1 + \frac{r^2}{L^2} - \frac{m}{r^2} + \frac{q^2}{r^4}, \quad g(r) = 1/f(r).$$

The metric possesses three Killing vectors  $\partial_t$ ,  $\partial_{\hat{\phi}}$ , and  $\partial_{\hat{\psi}}$ , where  $\hat{\phi} = \psi - \phi$ ,  $\hat{\psi} = \psi + \phi$ . For an equally rotating black hole, there are two additional Killing vectors [69, 70]

$$\cos \hat{\phi} \partial_{\hat{\theta}} - \cot \hat{\theta} \sin \hat{\phi} \partial_{\hat{\phi}} + \frac{\sin \hat{\phi}}{\sin \hat{\theta}} \partial_{\hat{\psi}}, \quad (14)$$

$$-\sin \hat{\phi} \partial_{\hat{\theta}} - \cot \hat{\theta} \cos \hat{\phi} \partial_{\hat{\phi}} + \frac{\cos \hat{\phi}}{\sin \hat{\theta}} \partial_{\hat{\psi}}, \quad (15)$$

where  $\hat{\theta} = 2\theta$ .

The event horizon is a well-defined boundary that is a null hypersurface and it comprises the outward null geodesics, which are not capable of hitting the null infinity in the future. The event horizon is a solution of  $F(r) = 0$ :

$$r_h^6 + L^2 r_h^4 + r_h^2 (j^2 m - L^2 m + 2L^2 q) + j^2 L^2 m - j^2 q^2 + L^2 q^2 = 0,$$

which is a cubic equation in  $r_h^2$ . The solutions are given by

$$r_{h,n}^2 = 2\sqrt{\frac{\frac{L^4}{3} + L^2 m - j^2 m - 2L^2 q}{3}} \cos \left[ \frac{1}{3} \arccos \left( \frac{2j^2 L^2 m - 3j^2 q^2 + \frac{2L^6}{9} + L^4 m - 2L^4 q + 3L^2 q^2}{2j^2 m - \frac{2L^4}{3} - 2L^2 m + 4L^2 q} \right) \right. \\ \left. \sqrt{\frac{3}{\frac{L^4}{3} + L^2 m - j^2 m - 2L^2 q}} - \frac{2\pi n}{3} \right], \quad n = 0, 1, 2, \quad (16)$$

which indicates that the black hole has two horizons because of the two real positive roots. The constants  $(m, q)$  are related to  $(M, Q)$  as given in Eq. (11). As  $j \rightarrow 0$ , the horizon radius reduces to the five-dimensional charged AdS black hole. For both  $q, j \rightarrow 0$ , we have the five-dimensional Schwarzschild AdS black hole. In addition to  $q, j \rightarrow 0$ , if we take  $L \rightarrow \infty$ , we have  $r_h^2 = m$ , which is the radius of the five-dimensional Schwarzschild-Tangherlini spacetime. We plot in Fig. 1, the Cauchy horizon (blue dashed line) and the event horizon (black solid lines) with respect to the variation of the charge parameter (left figure) and the rotation parameter (right figure), respectively. To show the parametric bounds on  $q$  and  $j$ , we plot the charge parameter  $q$  as a function of the rotation parameter in Fig. 2. The region below the red line corresponds to the allowed region, whereas the region above the red line is forbidden for the parameters representing the black holes.

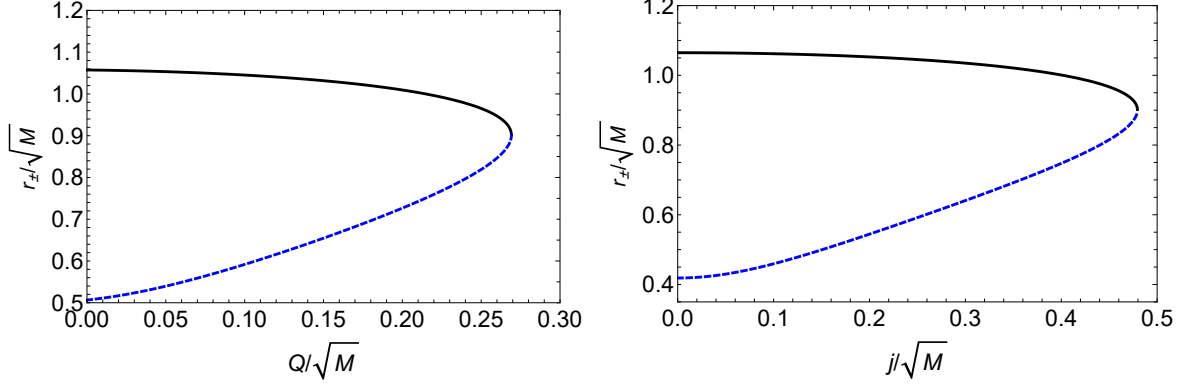


FIG. 1. The plot of the Cauchy horizon (blue dashed line) and the event horizon (black solid lines) vs the charge parameter  $Q$  for  $j = 0.1, L = 10$  (the left plot) and the rotation parameter  $j$  for  $Q = 0.1, L = 10$  (the right plot).

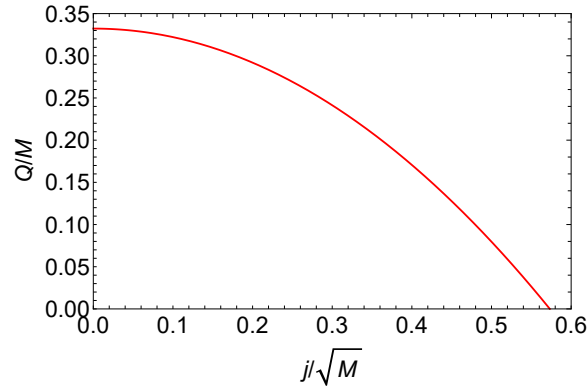


FIG. 2. The plot of the black hole charge parameter  $Q/M$  vs the rotation parameter  $j/\sqrt{M}$ . This is the parameter space in the plane  $(Q/M, j/\sqrt{M})$  for the CLP black hole. The red line represents the extremal black hole with degenerate Cauchy and the event horizons. The region above the red line is the no black hole region while the region below it corresponds to the black hole region.

### III. DEFLECTION ANGLE IN A FIVE-DIMENSIONAL CHARGED EQUALLY ROTATING BLACK HOLE WITH A COSMOLOGICAL CONSTANT

In this section, we discuss the deflection angle of light rays when they pass by a black hole. We also investigate the strong field gravitational lensing phenomena in the five-dimensional, charged equally rotating CLP black hole. We see the effect of the charge  $q$  and the rotation parameter  $j$ . For calculation simplicity, we restrict ourselves to the case of the equatorial plane,  $\theta = \frac{\pi}{2}$ .

Therefore, Eq. (7) reduces to

$$ds^2 = \left( -f(r) + \Sigma^2(r)\Omega^2(r)h(r) \right) dt^2 + g(r)dr^2 + \Sigma^2(r)h(r)d\psi^2 + \frac{1}{4}r^2\Sigma^2(r)d\phi^2 - 2\Sigma^2(r)h(r)\Omega(r)d\psi dt. \quad (17)$$

The components of the metric tensor are written in a more compact functional form as

$$\begin{aligned} g_{tt} &= \partial_t \cdot \partial_t = -f(r) + \Sigma^2(r)\Omega^2(r)h(r) = -A(r), \\ g_{rr} &= \partial_r \cdot \partial_r = g(r) = B(r), \\ g_{\phi\phi} &= \partial_\phi \cdot \partial_\phi = \frac{1}{4}r^2\Sigma^2(r) = C(r), \\ g_{\psi\psi} &= \partial_\psi \cdot \partial_\psi = \Sigma^2(r)h(r) = D(r), \\ g_{\psi t} &= \partial_t \cdot \partial_\psi = -\Sigma^2(r)\Omega(r)h(r) = g_{t\psi} = -H(r). \end{aligned} \quad (18)$$

We can rewrite Eq. (7) as

$$ds^2 = -A(r)dt^2 + B(r)dr^2 + C(r)d\phi^2 + D(r)d\psi^2 - 2H(r)dt d\psi. \quad (19)$$

It is to be mentioned here that the coordinate  $(t, r, \phi, \psi)$  are now rescaled to be  $t \rightarrow t/\sqrt{M}$ ,  $r \rightarrow r/\sqrt{M}$ ,  $\phi \rightarrow \phi/\sqrt{M}$ , and  $\psi \rightarrow \psi/\sqrt{M}$ . Similarly, the parameters defining the black hole are rescaled in a dimensionless way as follows:  $Q \rightarrow Q/M$ ,  $j \rightarrow j/\sqrt{M}$  and  $L \rightarrow L/\sqrt{M}$ . Therefore from now on, all the coordinates including the black hole parameters are understood as dimensionless quantities. The above *ansatz* has residual gauge freedom  $\psi \rightarrow \psi + \alpha t$  and  $\Omega \rightarrow \Omega + \alpha$ , here  $\Omega$  is the angular velocity and it is symmetric for  $t \rightarrow -t$ ,  $\phi \rightarrow \phi + 2\pi$  and  $\psi \rightarrow \psi + \pi$ . Killing vectors are  $\eta_t^\mu = \delta_t^\mu$ ,  $\eta_\phi^\mu = \delta_\phi^\mu$  and  $\eta_\psi^\mu = \delta_\psi^\mu$ . Equations of motion are

$$\begin{aligned} \mathcal{E} &= -g_{0\mu}x^{\dot{\mu}} = -g_{tt}\dot{t} - g_{t\psi}\dot{\psi} = A(r)\dot{t} + H(r)\dot{\psi}, \\ L_\phi &= g_{3\mu}x^{\dot{\mu}} = g_{\phi\phi}\dot{\phi} = C(r)\dot{\phi}, \\ L_\psi &= g_{4\mu}x^{\dot{\mu}} = g_{\psi\psi}\dot{\psi} + g_{\psi t}\dot{t} = D(r)\dot{\psi} - H(r)\dot{t}. \end{aligned} \quad (20)$$

Rearranging Eq. (20) we have

$$\begin{aligned} \dot{\psi} &= \frac{A(r)L_\psi + H(r)\mathcal{E}}{H^2(r) + A(r)D(r)}, \\ \dot{t} &= \frac{D(r)\mathcal{E} - H(r)L_\psi}{H^2(r) + A(r)D(r)}, \\ \dot{\phi} &= \frac{L_\phi}{C(r)}, \end{aligned} \quad (21)$$

whereas the radial null geodesic is obtained by using  $ds^2 = 0$

$$\dot{r}^2 = \frac{1}{B(r)} \left[ \frac{(D(r)\mathcal{E} - 2H(r)L_\psi)\mathcal{E} - A(r)L_\psi^2}{H^2(r) + A(r)D(r)} - \frac{L_\phi^2}{C(r)} \right]. \quad (22)$$



The geodesic equation of motion for  $\theta$  is

$$\frac{C'(r)}{2C(r)} \frac{d\theta}{d\lambda} \frac{dr}{d\lambda} - \frac{H(r) \sin \theta}{2C(r)} \frac{d\phi}{d\lambda} \frac{dt}{d\lambda} + \frac{\cos \theta \sin \theta (-C(r) + D(r))}{C(r)} \left( \frac{d\phi}{d\lambda} \right)^2 + \frac{D(r) \sin \theta}{2C(r)} \frac{d\psi}{d\lambda} \frac{d\phi}{d\lambda} = 0. \quad (23)$$

For  $\theta = \pi/2$ , Eq. (23) reduces to

$$\frac{d\phi}{d\lambda} \left( -H(r) \frac{dt}{d\lambda} + D(r) \frac{d\psi}{d\lambda} \right) = 0, \quad (24)$$

which gives us either  $\frac{d\phi}{d\lambda} = 0$ , i.e.,  $L_\phi = 0$  or  $L_\psi = \left( -H(r) \frac{dt}{d\lambda} + D(r) \frac{d\psi}{d\lambda} \right) = 0$ . In order to get the simpler results, we shall consider the case when  $L_\psi = 0$ , which means the total angular momentum of the photon  $J$  is equal to  $L_\phi$  and the effective potential  $V_{eff} = -\dot{r}^2$ , where  $\dot{r}^2$  under such conditions is given by

$$\dot{r}^2 = \frac{1}{B(r)} \left[ \frac{D(r)\mathcal{E}^2}{H^2(r) + A(r)D(r)} - \frac{L_\phi^2}{C(r)} \right]. \quad (25)$$

To compute the impact parameter, we use  $V_{eff} = 0$ ,

$$u = J = L_\phi / \mathcal{E} = \sqrt{\frac{C(r_0)D(r_0)}{H^2(r_0) + A(r_0)D(r_0)}}, \quad (26)$$

where  $u$  denotes the impact parameter. The variation of  $V_{eff}$  with respect to radial distance  $r$  is shown in Fig. 3 for different values of the impact parameter  $u$  at fixed  $Q$  and fixed  $j$  values. We observe that at  $u_s = u_{sc}$ , we have the critical impact parameter (red solid line), which depends on the parameters  $Q$  and  $j$ . At  $u_s = u_{sc}$  we have the unstable circular orbits along which the photon propagates. The photon orbit radius as a function of the charge  $Q$  and the rotation parameter  $j$  is depicted in Fig. 4. The photon orbit decreases quickly when plotted as a function of the charge  $Q$ . It decreases slowly for lower values of  $j$  and for higher values of  $j$ , the decrease in the photon orbit radius is enhanced. Similar is the case for the impact parameter, as shown in Fig. 5.

The equation of the circular orbit of a photon is obtained using  $V'_{eff} = 0$ ,

$$C(r_0) [D(r_0)^2 A'(r_0) - H(r_0)^2 D'(r_0) + 2D(r_0)H(r_0)H'(r_0)] - D(r_0)C'(r_0) [A(r_0)D(r_0) + H(r_0)^2] = 0. \quad (27)$$

where  $r_0$  is the closest of the photon spheres. Eqs. (26) and (27) are more complex than those in the usual spherical, symmetric black hole spacetime. As a limiting case, when the parameter  $j \rightarrow 0$ , we have  $H(r) \rightarrow 0$  and therefore, Eq. (27) has a much simpler form,

$$C(r_0)A'(r_0) - C'(r_0)A(r_0) = L^2 (4q^2 + 6qx + x(2x - 3)) + x^3 = 0, \quad x = r_0^2. \quad (28)$$

The above equation is cubic in nature and the roots are easily derivable as

$$x_k = 2\sqrt{-\frac{\mathcal{P}}{3}} \cos \left[ \frac{1}{3} \arccos \left( \frac{3\mathcal{Q}}{2\mathcal{P}} \sqrt{\frac{-3}{\mathcal{P}}} \right) - \frac{2\pi k}{3} \right], \quad k = 0, 1, 2, \quad (29)$$

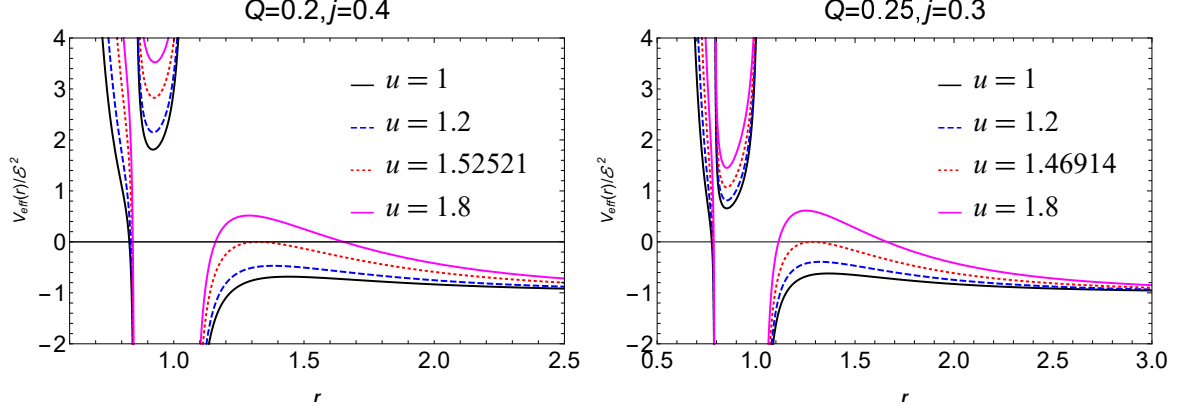


FIG. 3. The behaviour of the effective potential  $V_{eff}$  with respect to the dimensionless radial coordinate  $r$  for different values of the impact parameter  $u$ .

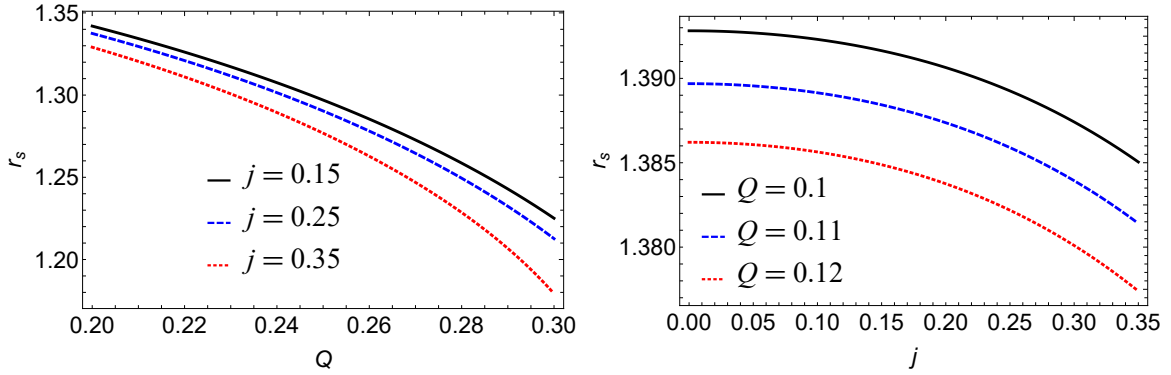


FIG. 4. The variations of the photon sphere radius  $r_s$  with respect to the charge parameter  $Q$  (the left plot) and the rotation parameter  $j$  (the right plot).

where  $\mathcal{P} = (6q - 3)L^2 - \frac{4L^4}{3}$ ,  $\mathcal{Q} = 4l^2q^2 + 2L^4(1 - 2q) - \frac{16L^6}{27}$ . Obviously, for  $q = 0$ , we have only one root that corresponds to  $x = \sqrt{L^2(L^2 + 3)} - L^2$ . However, we cannot determine the photon sphere radius analytically for  $j \neq 0$  so we have computed it numerically. The value of the impact parameter for  $j = 0$  is computed to be

$$\begin{aligned}
 u_s|_{j=0} &= \frac{L\mathcal{X}_3^2}{2\sqrt{3}\mathcal{X}_2^{1/3} \left( 27L^2q^2\mathcal{X}_2 + L^2\mathcal{X}_3^2 \left( 4L^2 - 18q + \mathcal{X}_2^{1/3} + 9 \right) + \mathcal{X}_3 \left( 4L^4\mathcal{X}_2^{2/3} - 2L^2\mathcal{X}_2 + \mathcal{X}_2^{4/3} \right) \right)}, \\
 \mathcal{X}_1 &= \sqrt{-3L^8(4q^2 - 36q + 9) - 81L^6(8q^2 - 6q + 1) + 324L^4q^4}, \\
 \mathcal{X}_2 &= -8L^6 + 27L^4(2q - 1) - 54L^2q^2 + 3\mathcal{X}_1, \\
 \mathcal{X}_3 &= 4L^4 + L^2(-18q - 2\mathcal{X}_2^{1/3} + 9) + \mathcal{X}_2^{2/3}.
 \end{aligned} \tag{30}$$

In Fig. 6 and Fig. 7, the variations of the photon orbits and the impact parameter as functions

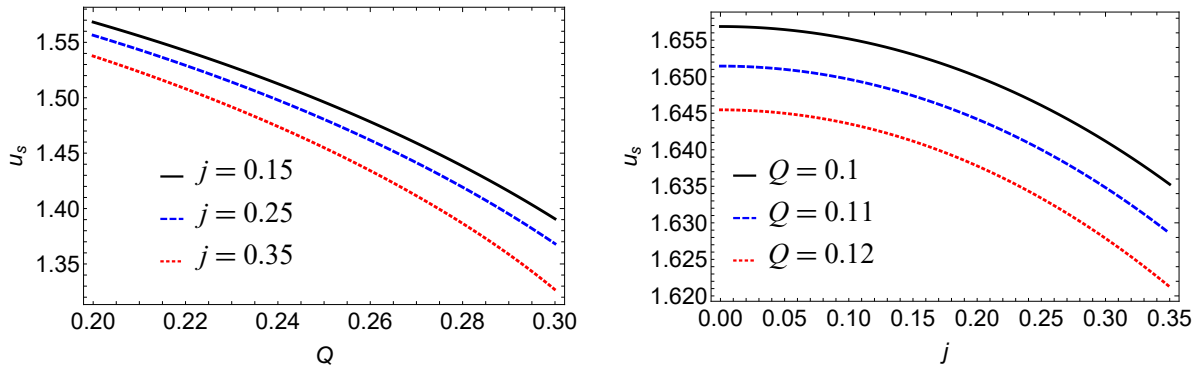


FIG. 5. The variations of the impact parameter  $u_s$  with respect to the charge parameter  $Q$  (the left plot) and the rotation parameter  $j$  (the right plot).

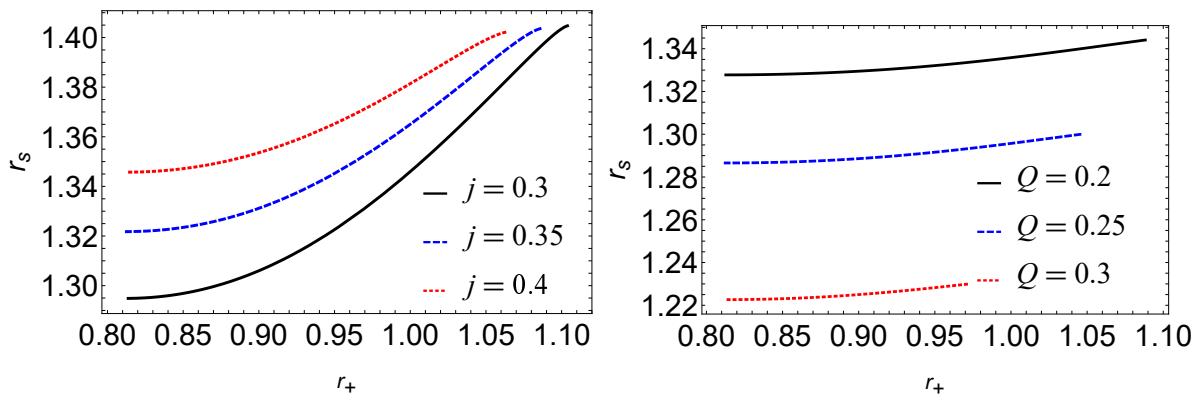


FIG. 6. The behaviour of the photon orbit  $r_s$  (in units of  $\sqrt{M}$ ) with respect to the horizon radius  $r_+$  (in units of  $\sqrt{M}$ ) for different values of the charge parameter with the fixed rotation parameter  $j = 0.1$  (the left plot) and different values of the rotation parameter with the fixed charge parameter  $Q = 0.1$  (the right plot).

of the horizon radius for a fixed  $Q$  (left) and a fixed  $j$  value (right) are shown, respectively. For the fixed  $Q$  value, the variation of the photon orbits as well as the impact parameter is almost constant, but the gap of the plots is highly sensitive to the  $j$  value. For a fixed  $j$  value, the variations of both  $r_s$  and  $u_s$  are monotonically varying functions of the horizon radius. They increase as the horizon's radius increases. For vanishing angular momentum, i.e., for  $j = 0$ , we have the exact expression for the photon orbits, Eq. (29) and the minimum impact parameter, Eq. (30). We observe that, as in the four-dimensional Kerr black hole spacetime, the value of the unstable circular orbit is dependent on the photon winding number in the direction of the black hole rotation ( $j > 0$ ) or in the opposite direction of the black hole rotation (i.e.,  $j < 0$ ). It is also emphasized that for the Kaluza-Klein rotating black hole with squashed horizons, the unstable circular orbits are independent of the black hole rotation, as the rotation parameter appears to be an even power of  $j^2$ .

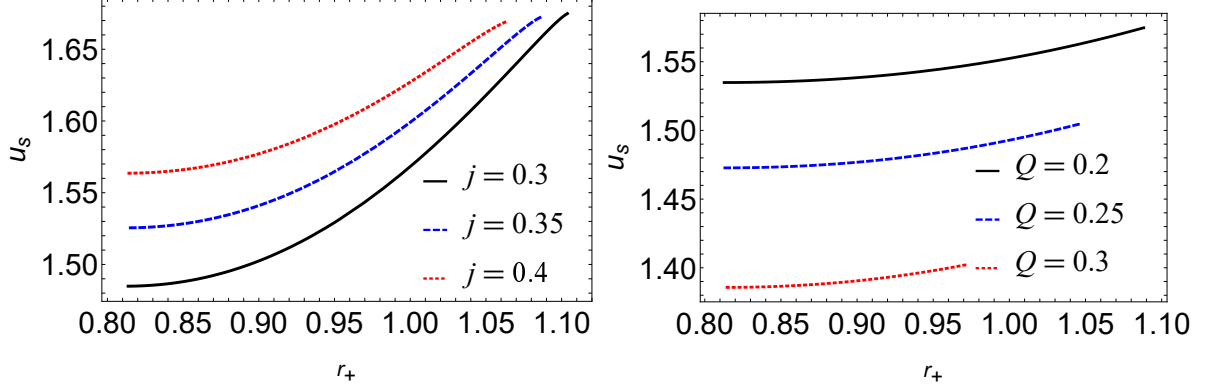


FIG. 7. The behaviour of the impact parameter  $u_s$  (in units of  $\sqrt{M}$ ) with respect to the horizon radius  $r_+$  (in units of  $\sqrt{M}$ ) for different values of the charge parameter with the fixed rotation parameter  $j = 0.1$  (left) and for different values of the rotation parameter with the fixed charge parameter  $Q = 0.1$  (right).

Since  $\dot{r}^2$  vanishes at the closest distance  $r = r_0$ , from the trajectory equation we have

$$A(r_0)\dot{t}_0^2 + 2H(r_0)^2\dot{t}_0\dot{\psi}_0 = C(r_0)\dot{\phi}_0^2 + D(r_0)\dot{\psi}_0^2, \quad (31)$$

Using Eq. (22), we have

$$\dot{r} = \frac{dr}{d\lambda} = \frac{1}{\sqrt{B(r)F(r_0)F(r)}} \sqrt{F(r_0) - \frac{C(r_0)F(r)}{C(r)}}. \quad (32)$$

The radial motion of the photon is governed by

$$\frac{d\phi}{dr} = \frac{\sqrt{B(r)F(r_0)F(r)}}{C(r)} \frac{1}{\sqrt{F(r_0) - \frac{C(r_0)F(r)}{C(r)}}} \quad (33)$$

and

$$\frac{d\psi}{dr} = \frac{H(r)}{D(r)} \sqrt{\frac{B(r)F(r_0)}{F(r)}} \frac{1}{\sqrt{F(r_0) - \frac{C(r_0)F(r)}{C(r)}}} \quad (34)$$

with

$$F(r) = \frac{H^2(r) + A(r)D(r)}{D(r)}. \quad (35)$$

The deflection angles  $\psi$  and  $\phi$  for the photon coming from the infinite can be expressed as [17]

$$I_\psi(r_0) = 2 \int_{r_0}^{\infty} \frac{d\psi}{dr} dr = 2 \int_{r_0}^{\infty} dr \frac{H(r)}{D(r)} \sqrt{\frac{B(r)F(r_0)}{F(r)}} \frac{1}{\sqrt{F(r_0) - \frac{C(r_0)F(r)}{C(r)}}}, \quad (36)$$

$$I_\phi(r_0) = 2 \int_{r_0}^{\infty} \frac{d\phi}{dr} dr = 2 \int_{r_0}^{\infty} dr \frac{\sqrt{B(r)F(r_0)F(r)}}{C(r)} \frac{1}{\sqrt{F(r_0) - \frac{C(r_0)F(r)}{C(r)}}}. \quad (37)$$

Except for the metric function  $H(r)$  which is an odd function of the rotation parameter, the other functions contain an even power of the rotation parameter. Therefore, the deflection angle corresponding to the  $\phi$ -angle is dependent on whether the black hole is in retrograde or in prograde motion. However, the deflection angle related to the angle  $\psi$  is an even function of the rotation parameter  $j$ , which means that it does not matter whether the photon is winding in the direction of the black hole rotation or in the converse direction, the deflection angle is always independent of the black hole rotation. Furthermore, unlike the four-dimensional case, in the equatorial plane ( $\theta = \pi/2$ ), the rotation of the black hole is in the  $\psi$  direction rather than in the  $\phi$  direction, which is evident from the expression of the spacetime as is given in Eq. (19), where the only cross-term is  $dt d\psi$ . This also clarifies the fact that the gravitational lensing of the charged rotating black hole in five dimensions is not the same as the strong lensing phenomena of the usual four-dimensional Kerr or the Kerr-Newman black hole.

On defining  $z = 1 - \frac{r_0}{r}$ , we have

$$I_\phi(r_0) = \int_0^1 R(z, r_0) f(z, r_0) dz \quad (38)$$

with

$$R(z, r_0) = 2 \frac{r^2}{r_0 C(r)} \sqrt{B(r) F(r) C(r_0)} = P_1(r, r_0), \quad (39)$$

$$f(z, r_0) = \frac{1}{\sqrt{F(r_0) - F(r) C(r_0) / C(r)}} = P_2(r, r_0). \quad (40)$$

The function  $R(z, r_0)$  is regular for all values of  $z$  and  $r_0$ . From Eq. (40), we find that  $f(z, r_0)$  diverges as  $z$  tends to zero, i.e., as the photon approaches the marginally circular photon orbit. Therefore, we can split the integral Eq. (38) into divergent part  $I_D(r_0)$  and the regular one  $I_R(r_0)$

$$I_{D,\phi}(r_0) = \int_0^1 R(0, r_s) f_0(z, r_0) dz, \quad (41)$$

$$I_{R,\phi}(r_0) = \int_0^1 [R(z, r_0) f(z, r_0) - R(0, r_s) f_0(z, r_0)] dz. \quad (42)$$

We can expand the argument of the square root in  $f(z, r_0)$  to the second order in  $z$

$$f_0(z, r_0) = \frac{1}{\sqrt{p(r_0)z + g(r_0)z^2}} \quad (43)$$

with

$$p(r_0) = \frac{r_0}{C(r_0)} [C'(r_0)F(r_0) - C(r_0)F'(r_0)], \quad (44)$$

$$g(r_0) = \frac{r_0^2}{2C(r_0)} [2C'(r_0)C(r_0)F'(r_0) - 2C'(r_0)^2 F(r_0) + F(r_0)C(r_0)C''(r_0) - C^2(r_0)F''(r_0)].$$

To obtain Eq. (43) and Eq. (44) we expanded  $f(z, r_0)$  around  $z = 0$  upto order  $z^2$ . If we use Eq. (27), one obtains  $F(r)C'(r) = C(r)F'(r)$  which leads to  $p(r_0) = 0$  and  $r_s$  is the largest root of  $p(r_0)$ . This means that the leading term of the divergence in  $f_0(z, r_0)$  is  $z^{-1}$  and the integral Eq. (38) diverges logarithmically. Thus, in the strong field region, the deflection angle in the direction can be approximated very well as [17]:

$$\alpha_{D,\phi}(\theta) = -\bar{a} \log \left( \frac{\theta D_{OL}}{u_s} - 1 \right) + \bar{b} + O(u - u_s), \quad (45)$$

where

$$\begin{aligned} \bar{a} &= \frac{R(0, r_s)}{2\sqrt{g(r_s)}}, \\ \bar{b} &= -\pi + b_R + \bar{a} \log \frac{r_s^2 [C''(r_s)F(r_s) - C(r_s)F''(r_s)]}{u_s F(r_s) \sqrt{F(r_s)C(r_s)}}, \\ b_R &= I_R(r_s), \quad u_s = \sqrt{\frac{C(r_s)}{F(r_s)}}. \end{aligned} \quad (46)$$

Here the quantity  $D_{OL}$  is the distance between observer and gravitational lens,  $\theta = u/D_{OL}$  is the angular separation between the lens and the image. The subscript “s” represents the evaluation at  $r = r_s$ . Likewise, we can compute the corresponding  $\psi$  following Eq. (38). We can write

$$I_\psi(r_0) = \int_0^1 S(z, r_0) f(z, r_0) dz \quad (47)$$

with  $f(z, r_0)$  given by Eq. (40) and  $S(z, r_0)$  as

$$S(z, r_0) = 2 \frac{r^2 H(r)}{r_0 D(r)} \sqrt{\frac{B(r)F(r_0)}{F(r)}}. \quad (48)$$

The function  $S(z, r_0)$  is regular for all values of  $z$  and  $r_0$ . Whereas  $f(z, r_0)$  is divergent as for the case of  $I_{D,\phi}(r_0)$ , and we can follow the same expansion as well but replace  $\bar{a}$  with  $\bar{a}_\psi$ ,

$$\bar{a}_\psi = \frac{S(0, r_s)}{2\sqrt{g(r_s)}}, \quad (49)$$

$$I_{D,\psi}(r_0) = \int_0^1 S(0, r_s) f_0(z, r_0) dz, \quad (50)$$

$$I_{S,\psi}(r_0) = \int_0^1 [S(z, r_0) f(z, r_0) - R(0, r_s) f_0(z, r_0)] dz. \quad (51)$$

The study of the deflection angle only in the  $\phi$  direction would be focused on our recent purpose since it helps in observing real astronomical observations. One can likewise determine the integration regarding the strong lensing deflection angle in the  $\psi$  direction, which we denote by  $I_{\psi(r_0)}$ . This term also has the coefficients, which likely have the form of  $\bar{a}$  and  $\bar{b}$  but differ slightly. We should mention that the deflection angle in the  $\phi$ -direction also has a term that diverges logarithmically. Nevertheless, it should not be used in determining the strong deflection phenomena

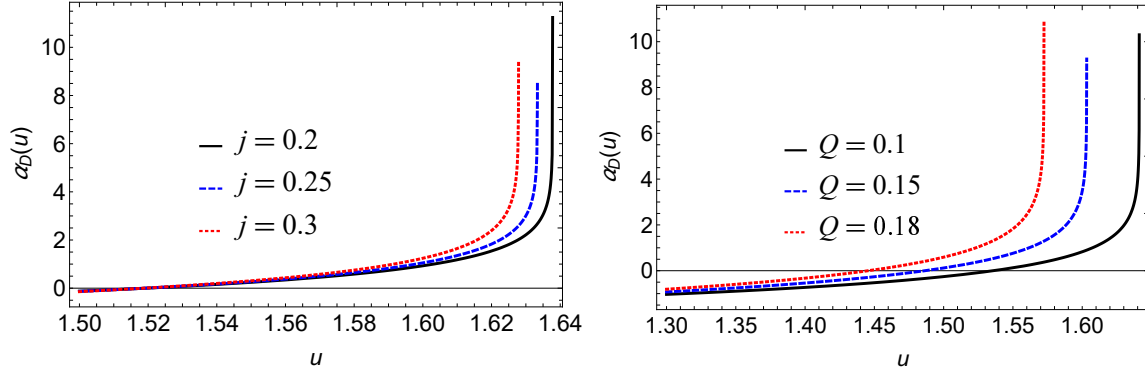


FIG. 8. The variation of the deflection angle  $\alpha_D(u)$  with respect to the impact parameter  $u$ . We have set  $Q = 0.12$  in the left plot and  $j = 0.3$  in the right one.

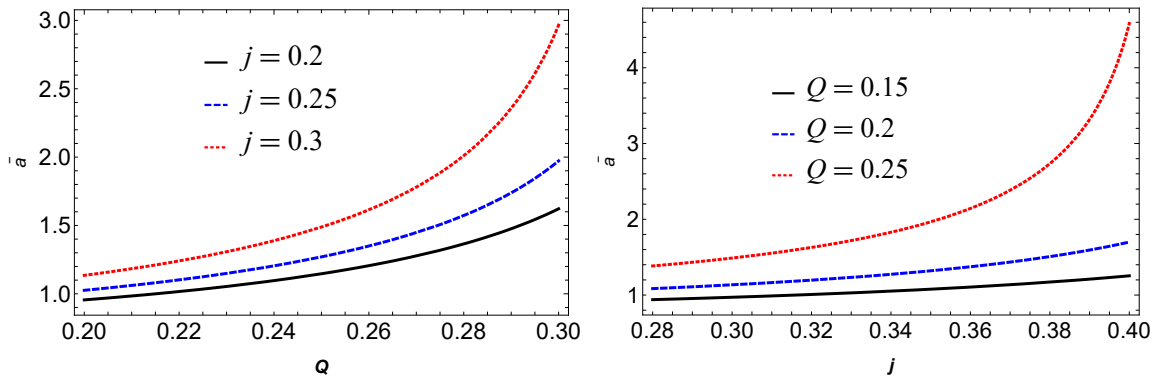


FIG. 9. The variations of the deflection coefficient  $\bar{\alpha}$  with respect to the charge parameter  $Q$  (the left plot) and the rotation parameter  $j$  (the right plot).

from observational perspectives. In Fig. 8, we plot the deflection angle with respect to the impact parameter for different values of the rotation parameter  $j$  (the left figure) and the charge parameter  $Q$  (the right figure). We can see from the figure that the deflection angle increases monotonically with the critical impact parameter  $u$  and diverges for large  $u$ . Similarly, the variations of the coefficients  $\bar{\alpha}$  and  $\bar{b}$  with respect to the rotation parameter and the charge parameter are shown in Fig. 9 and Fig. 10, respectively. We observe a monotonic variation for the coefficient  $\bar{\alpha}$  it increases with increasing  $Q$  and  $j$ , whereas the coefficient  $\bar{b}$  increases with  $Q$  but decreases with  $j$ .

#### IV. OBSERVABLES AND RELATIVISTIC IMAGES

The description of the gravitational lensing phenomena is determined through the lens equation. Many methods for calculating the lens equation depend on the choice of parameters we are interested in. In our calculation, we choose the gravitational lens, where the black hole is placed

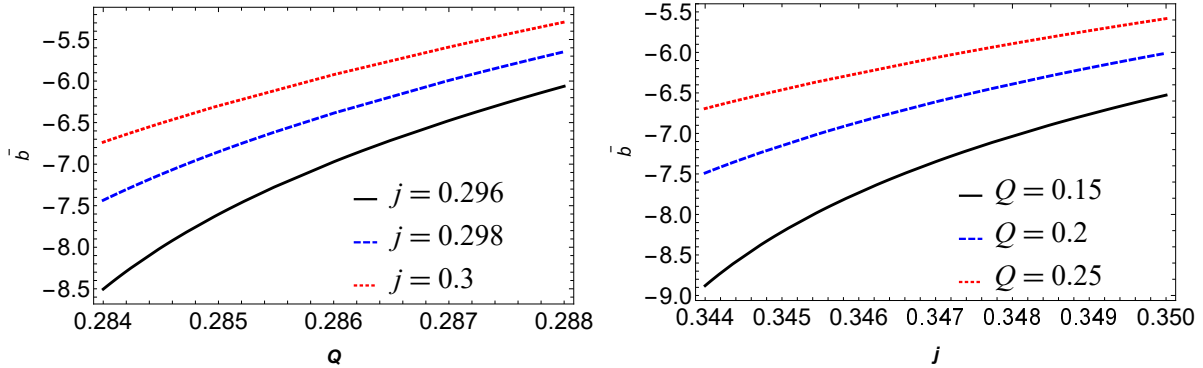


FIG. 10. The variations of the deflection coefficient  $\bar{b}$  with respect to the charge parameter  $Q$  (the left plot) and the rotation parameter  $j$  (the right plot).

in the middle of the configuration so that the observer is situated at one side, and the illuminating source of light is at another side. The light rays emanate from the source (S) and their actual paths are deviated due to the presence of the central black hole with high curvature. Then after making one or more windings, the light rays finally reach the observer position (O). In the picture of the black hole lens, the optical axis OL is the line connecting the black hole, the observer and the image, which will deviate at an angle  $\theta$  with respect to OL. On the other hand, the illuminating source of light is oriented at an angle  $\beta$  with respect to OL. The light emanating by the source is detected by the observer by an angle  $\alpha_D(\theta)$ .

Among various mathematical formulations, the method given by Ohanian was mostly used in the literature as the lens equation [25] to approximate the position of the source, lens and observer:

$$\xi = \frac{D_{OL} + D_{LS}}{D_{LS}}\theta - \alpha_D(\theta). \quad (52)$$

The angle  $\xi \in [-\pi, \pi]$  is used for the optical axis and the source orientations, whereas  $D_{OL}$  is the distance connecting the source and the observer, and  $D_{LS}$  is the line between the source and lens. The angles  $\xi$  and  $\beta$  are found to follow the relation [25, 31]

$$\frac{D_{OL}}{\sin(\xi - \beta)} = \frac{D_{LS}}{\sin \beta}. \quad (53)$$

For the completeness of the calculations and to have physical realization, the angles  $\theta$ ,  $\xi$ , and  $\beta$  are considered to be smaller because the formation of the relativistic images are dominant feature of the strong lensing phenomena. The light emanating from the source encounters the black hole and makes many winding or loops before it leaves such that the deflection angle  $\alpha$  is framed as  $2n\pi + \Delta\alpha_n$ , where  $n \in \mathbb{N}$  is an integer and is accounted for the loop counting and  $0 < \Delta\alpha_n \ll 1$ . Therefore, following Eq. (52) along with Eq. (53), for the smaller values of  $\theta$ , we have the lens



equation

$$\beta = \theta - \frac{D_{LS}}{D_{OL} + D_{LS}} \Delta\alpha_n. \quad (54)$$

We can use Eq. (54) to know information about the image formation. We know that when the impact parameter  $u \rightarrow u_s$ , the deflection angle  $\alpha_D(\theta)$  becomes divergent. Therefore, for each loop formed during the winding near the event horizon of the black hole, we certainly have one  $u_s$  at which the light rays reach from the lens to the observer. Accordingly, we have infinitely many images that are formed on both sides of the black hole. Now Eq. (45) together with  $\alpha_D(\theta_n^0) = 2n\pi$  is rewritten as

$$\theta_n^0 = \frac{u_s}{D_{OL}}(1 + e_n), \quad (55)$$

where

$$e_n = e^{\frac{\bar{b}-2n\pi}{a}}. \quad (56)$$

Now a Taylor series expansion of  $\alpha_D(\theta)$  around  $\theta_n^0$  up to first order in  $(\theta - \theta_n^0)$  may be approximated as [31]

$$\alpha_D(\theta) = \alpha_D(\theta_n^0) + \left. \frac{\partial\alpha_D(\theta)}{\partial\theta} \right|_{\theta_n^0} (\theta - \theta_n^0) + \mathcal{O}(\theta - \theta_n^0)^2. \quad (57)$$

Using Eq. (55) along with the condition  $\Delta\theta_n = \theta - \theta_n^0$ , we have the difference of the deflection angle

$$\Delta\alpha_n = -\frac{\bar{a}D_{OL}}{u_s e_n} \Delta\theta_n. \quad (58)$$

Therefore, the final lens equation Eq. (54) is approximated to be [31]

$$\beta = \theta_n^0 + \Delta\theta_n + \frac{D_{LS}}{D_{OL} + D_{LS}} \left( \frac{\bar{a}D_{OL}}{u_s e_n} \Delta\theta_n \right). \quad (59)$$

We ignore the second term in Eq. (59) since its contribution is very less in comparison to other terms, and then by substituting  $\Delta\theta_n = (\theta - \theta_n^0)$ , we have the  $\theta$ -equation for the  $n$ -th image as

$$\theta_n = \theta_n^0 + \frac{D_{OL} + D_{LS}}{D_{LS}} \frac{u_s e_n}{\bar{a}D_{OL}} (\beta - \theta_n^0). \quad (60)$$

Next, we discuss the creation and subsequent formation of Einstein's ring. Among many exotic features of the lensing phenomenon, the formation of Einstein's ring is the most striking one. When the light source, lens, and observer are aligned in a most suitable way so that the whole lens system

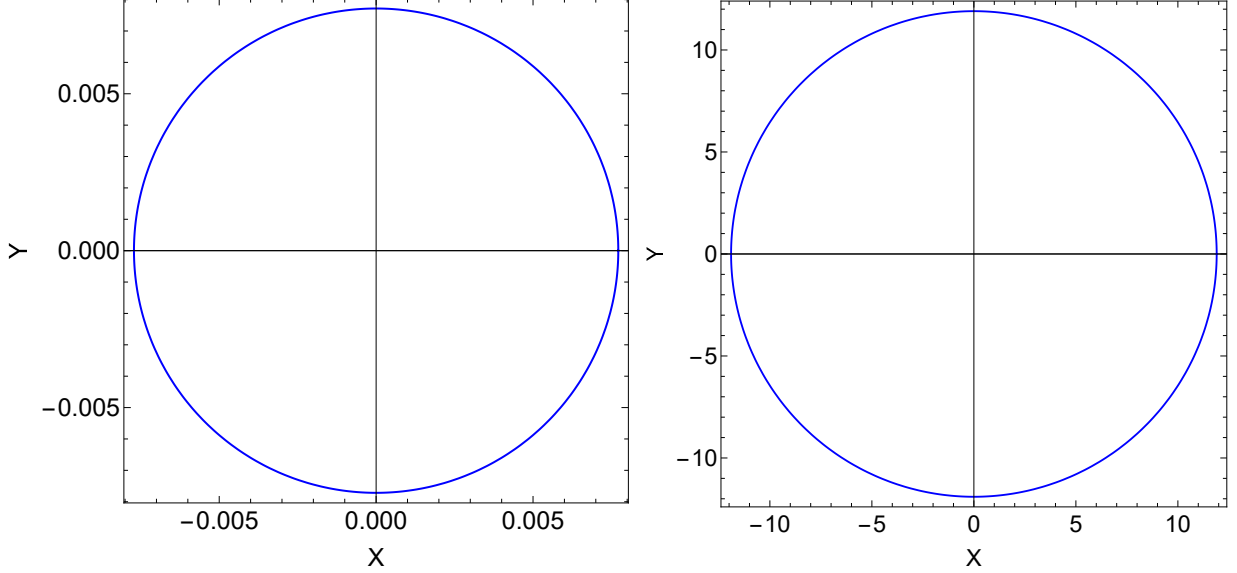


FIG. 11. Plots of the outermost Einstein rings for the black holes at the centre of nearby galaxies in the framework of the Schwarzschild geometry. The left plot corresponds to the *SgrA\** and the right one to that of *M87* [31].

plays a role in the formation of complex multiple images [25–27]. We also have double Einstein’s ring [74] formed depending on the source we have. For relativistic Einstein’s ring formation, the deflection angle  $\alpha$  must have a value greater than  $2\pi$ . For perfect alignment of the lens and the observer, we must set  $\beta = 0$ , so that the lens is situated at the middle of the line connecting the source and the observer. Therefore, Eq. (60) reduces to [31]

$$\theta_n^E = \left(1 - \frac{2u_s e_n}{D_{OL}\bar{a}}\right) \cdot \left(\frac{u_s}{D_{OL}}(1 + e_n)\right). \quad (61)$$

As a limiting case when  $D_{OL} \gg u_s$ , the angular radius Eq. (61) for Einstein’s ring reduces to

$$\theta_n^E = \frac{u_s}{D_{OL}} (1 + e_n), \quad (62)$$

where  $\theta_1^E$  represents the angular position of the outermost Einstein’s ring. In Fig. 11, we plot the angular position  $\theta_1^E$  of the supermassive black holes *SgrA\** and *M87*. Likewise, we get the image magnification which mathematically represents the ratio of the solid angle formed due to the image and the source with the lens. For the  $n$ th image formed, the magnification is expressed as [17, 19]

$$\mu_n = \frac{1}{\beta} \left[ \frac{u_s}{D_{OL}} (1 + e_n) \left( \frac{D_{OS}}{D_{LS}} \frac{u_s e_n}{D_{OL}\bar{a}} \right) \right]. \quad (63)$$

As the value  $n$  increases, the magnification decreases and accordingly, the image becomes fainter. We have another important quantity, the angular separation  $s$ , which is the angular difference

between the first and last image formed. Therefore, we have the important quantities of the relativistic images formed for a generic asymmetric rotating black hole as follows [17]

$$\theta_\infty = \frac{u_s}{D_{OL}}, \quad (64)$$

$$s = \theta_1 - \theta_\infty \approx \theta_\infty (e^{\frac{b-2\pi}{a}}), \quad (65)$$

$$r_{\text{mag}} = \frac{\mu_1}{\sum_{n=2}^{\infty} \mu_n} \approx e^{\frac{2\pi}{a}}. \quad (66)$$

These observables are plotted in a realistic scenario for supermassive black holes such as Sgr A\* and M87 [73] in Fig. 12 and Fig. 13. The details of mass and other parameters for Sgr A\* [75] are:  $M = 4.3 \times 10^6 M_\odot$  and  $d = 8.35$  Kpc, while for M87 [12],  $M = 6.5 \times 10^9 M_\odot$  and  $d = 16.8$  Mpc.

## V. TIME DELAY IN THE STRONG FIELD LIMIT

In this section, we derive the time required for the photon or light to go from  $r_0$  to  $r$  or from  $r$  to  $r_0$ . We follow an approach similar to the one reported in the previous subsection for the deflection angle but with some subtraction strategies to treat the integrals. For more details, see Refs. [76–78].

For an observer at infinity, the time taken from the photon to travel from the source to the observer is given by

$$T = \int_{t_0}^{t_f} dt. \quad (67)$$

Next, we change the integration variable from  $t$  to  $r$  and split the integral into two phases (approaching and leaving):

$$T = \int_{D_{LS}}^{r_0} \frac{dt}{dr} dr + \int_{r_0}^{D_{OL}} \frac{dt}{dr} dr. \quad (68)$$

Utilising the symmetry between approach and departure, we can combine the two integrals by extending the integration limits to infinity. This can be accomplished by subtracting two terms, given by

$$T = 2 \int_{r_0}^{\infty} \left| \frac{dt}{dr} \right| dr - \int_{D_{OL}}^{\infty} \left| \frac{dt}{dr} \right| dr - \int_{D_{LS}}^{\infty} \left| \frac{dt}{dr} \right| dr. \quad (69)$$

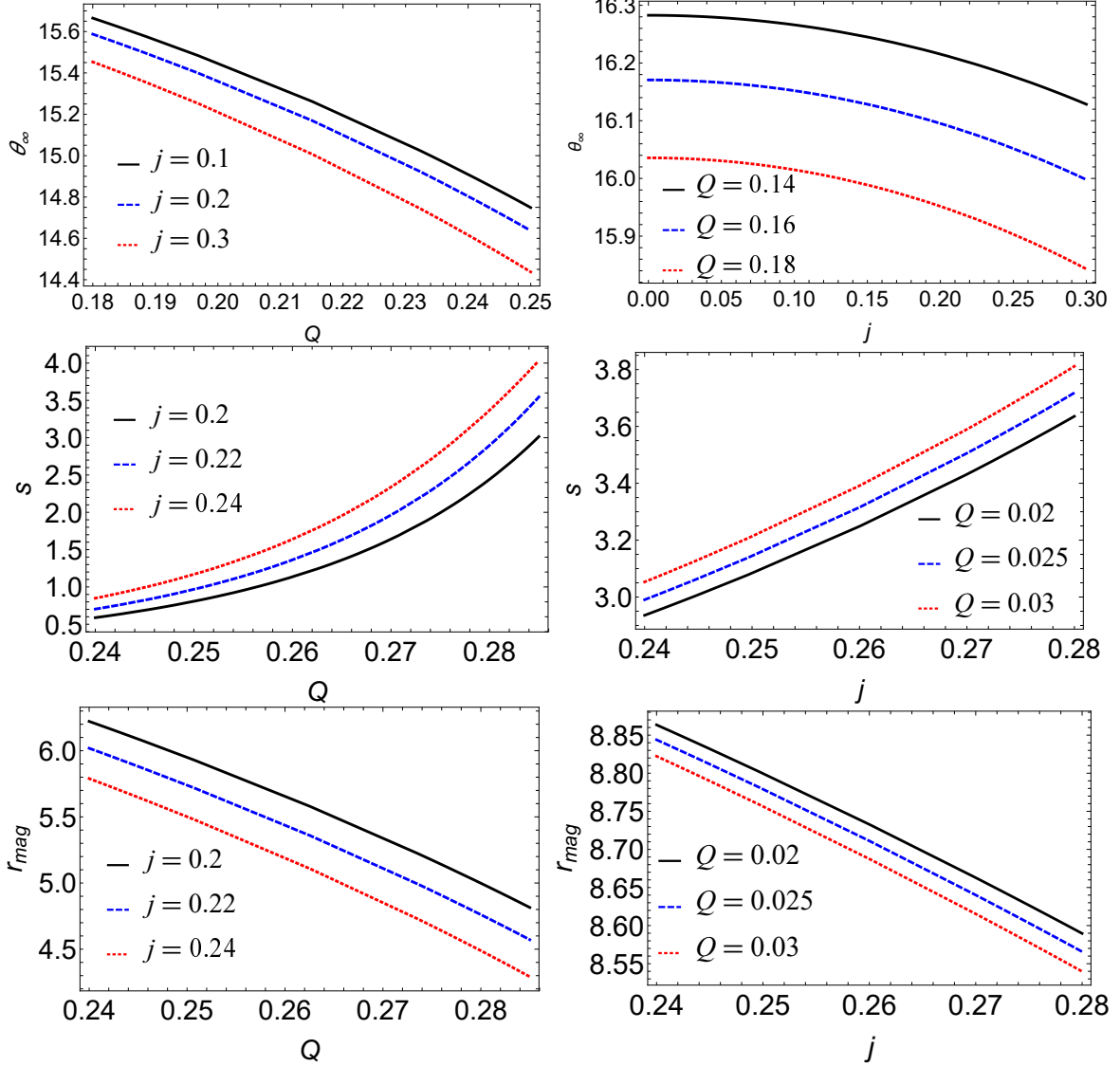


FIG. 12. Plot of the lensing variables for Sgr A\* with respect to the charge parameter  $Q$  (the left plot) and the rotation parameter  $j$  (the right plot).

If we consider two photons travelling on different trajectories, the time delay between them is

$$\begin{aligned}
T_1 - T_2 = & 2 \int_{r_{0,1}}^{\infty} \left| \frac{dt}{dr} (r, r_{0,1}) \right| dr - 2 \int_{r_{0,2}}^{\infty} \left| \frac{dt}{dr} (r, r_{0,2}) \right| dr \\
& - \int_{D_{OL}}^{\infty} \left| \frac{dt}{dr} (r, r_{0,1}) \right| dr + \int_{D_{OL}}^{\infty} \left| \frac{dt}{dr} (r, r_{0,2}) \right| dr \\
& - \int_{D_{LS}}^{\infty} \left| \frac{dt}{dr} (r, r_{0,1}) \right| dr + \int_{D_{LS}}^{\infty} \left| \frac{dt}{dr} (r, r_{0,2}) \right| dr.
\end{aligned} \tag{70}$$

Supposing that the observer and the source are very far from the black hole,  $dt/dr$  is effectively 1 in the last four integrals, which thus exactly cancel each other. We are thus left with the first two integrals.

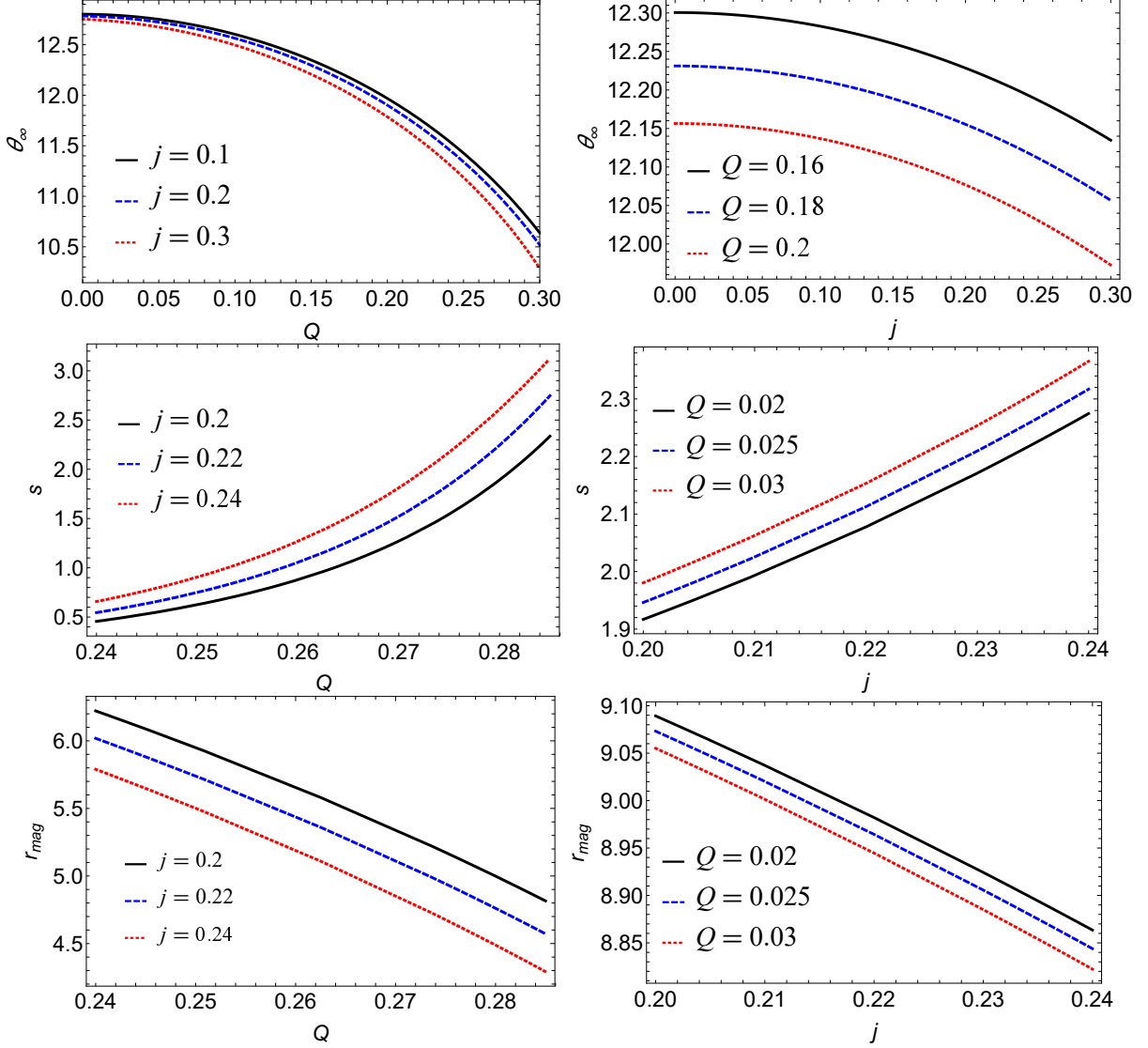


FIG. 13. Plot of the lensing variables for M87 with respect to the charge parameter  $Q$  (the left plot) and the rotation parameter  $j$  (the right plot).

Dividing Eq. (21) by Eq. (25), we obtain

$$\frac{dt}{dr} = \tilde{P}_1(r, r_0) P_2(r, r_0), \quad (71)$$

where

$$\tilde{P}_1(r, r_0) = \sqrt{\frac{B(r)F(r_0)}{F(r)}}, \quad (72)$$

and  $P_2$  is defined by Eq. (40). It can be seen that  $dt/dr$  tends to one at large  $r$  limit, and the two integrals in Eq. (70) are separately divergent, while their difference is finite. The time delay results from the different paths the photons follow while they wind around the black hole. When

the two photons are far from the black hole,  $dt/dr \rightarrow 1$  and the two integrals compensate each other. Separating the two regimes, we can write individually convergent integrals. To achieve this, we subtract and add the function  $\tilde{P}_1(r, r_{0,i})/\sqrt{F_{0,i}}$  to each integrand. Supposing  $r_{0,1} < r_{0,2}$ , we can write

$$\begin{aligned} T_1 - T_2 = & \tilde{T}(r_{0,1}) - \tilde{T}(r_{0,2}) + 2 \int_{r_{0,1}}^{r_{0,2}} \frac{\tilde{P}_1(r, r_{0,1})}{\sqrt{F_{0,1}}} dr \\ & + 2 \int_{r_{0,2}}^{\infty} \left[ \frac{\tilde{P}_1(r, r_{0,1})}{\sqrt{F_{0,1}}} - \frac{\tilde{P}_1(r, r_{0,2})}{\sqrt{F_{0,2}}} \right] dr, \end{aligned} \quad (73)$$

where

$$\tilde{T}(r_0) = \int_0^1 \tilde{R}(z, r_0) f(z, r_0) dz, \quad (74)$$

$$\tilde{R}(z, x_0) = \frac{2r^2}{r_0} \tilde{P}_1(r, r_0) \left( 1 - \frac{1}{\sqrt{F_{0,f}(z, r_0)}} \right), \quad (75)$$

and  $f(z, r_0)$  is defined by Eq. (40). We can verify that Eq. (73) is similar to Eq. (70) by substituting all the formulas, but now it is expressed as the sum of independently convergent integrals.

In actuality, the time taken by the light ray to wind around the black hole is represented by the integral  $\tilde{T}(r_0)$ . We have deducted a term from the definition of  $R(z, r_0)$  that is negligible when the photon is near the black hole but cancels the integrand when the photon is distant from the black hole in order to cut off the integrands at large  $r$  values. As we shall see in a moment, the residual terms of this subtraction are often subleading with respect to  $\Delta\tilde{T}$  and are kept in the final two integrals of Eq. (73).

The integral Eq. (75) can be solved following the same technique of the integral (38), just replacing  $R$  by  $\tilde{R}$ . The result is

$$\tilde{T}(u) = -\tilde{a} \log\left(\frac{u}{u_s} - 1\right) + \tilde{b} + O(u - u_s), \quad (76)$$

where  $u_s$  is defined by Eq. (46) and

$$\tilde{a} = \frac{\tilde{R}(0, r_s)}{2\sqrt{q(r_s)}}, \quad (77)$$

$$\tilde{b} = -\pi + \tilde{b}_R + \tilde{a} \log \frac{r_s^2 [C'''(r_s)F(r_s) - C(r_s)F''(r_s)]}{u_s F(r_s) \sqrt{F(r_s)} C(r_s)} \quad (78)$$

with

$$\tilde{b}_R = \int_0^1 \left[ \tilde{R}(z, r_s) f(z, r_s) - \tilde{R}(0, r_s) f_0(z, r_s) \right] dz. \quad (79)$$

We have shown the variation of  $\tilde{T}(u)$  with respect to  $u$  for different  $j$  and  $Q$  values in Fig. 14. Next, the variations of  $\tilde{a}$  and  $\tilde{b}$  with respect to the parameters  $Q$  and  $j$  are shown in Fig. 15 and Fig. 16, respectively.

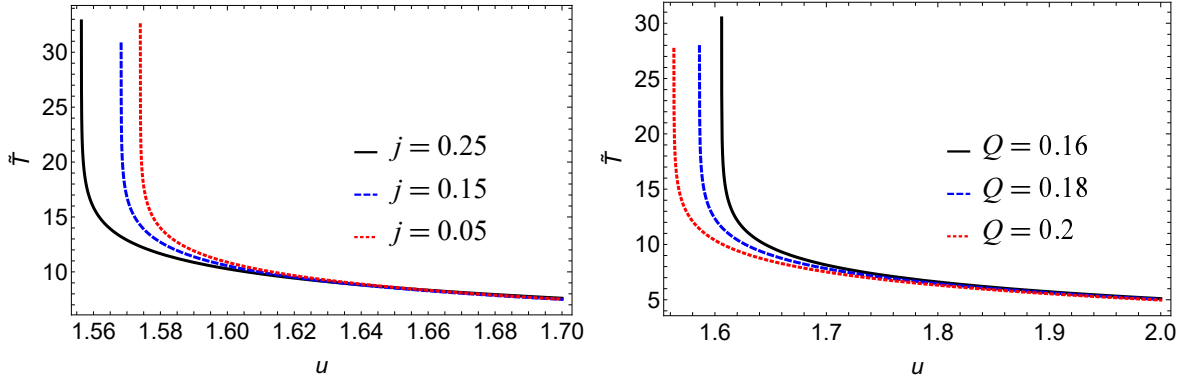


FIG. 14. Plot of the variation of  $\tilde{T}(u)$  with respect to the parameter  $u$  for different values of the rotation parameter  $j$  (the left plot) and constant value of the charge parameter  $Q$  (the right plot).

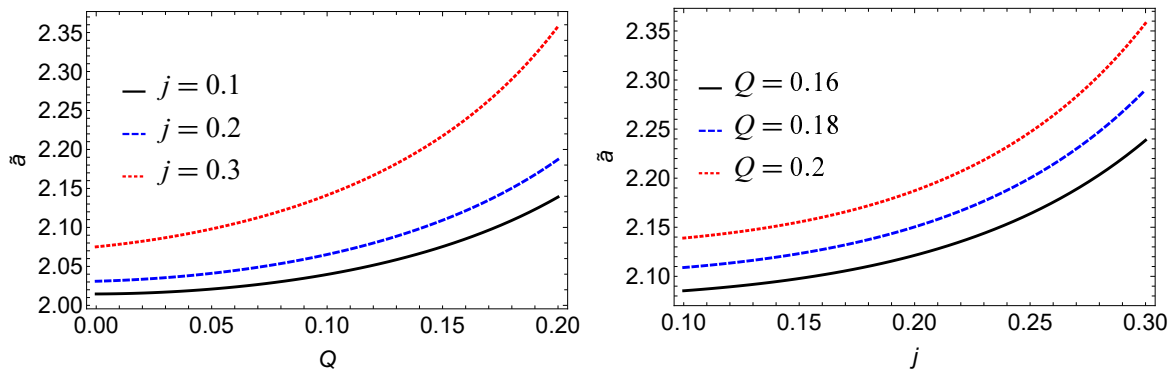


FIG. 15. Plot of the variation of  $\tilde{a}$  with respect to the charge parameter  $Q$  (the left plot) and the rotation parameter  $j$  (the right plot).

## VI. CONCLUSION

The strong gravitational lensing provides a very powerful tool to probe the nature of black holes in different modified theories of gravity. In addition, the extra dimension is a promising entity that helps us in determining a unified nature of the theory of everything. We have investigated the strong gravitational lensing in the equatorial plane ( $\theta = \pi/2$ ) of the five-dimensional charged equally rotating black hole in the presence of a negative cosmological constant. The presence of an additional factor of  $dt d\psi$  term in the spacetime metric itself, even for the equatorial plane, accounts for the extra dimension. We observed systematically the effects of the rotation and the charge parameters on the circular photon sphere radius for a fixed value of the curvature radius. The strong deflection angle and the coefficients  $\bar{a}$ ,  $\bar{b}$  were plotted in order to show the role of the black hole parameters. We found that the coefficient  $\bar{a}$  increases with the charge parameter, while it decreases or increases with the rotation parameter  $j$ , depending upon the choice of the values of

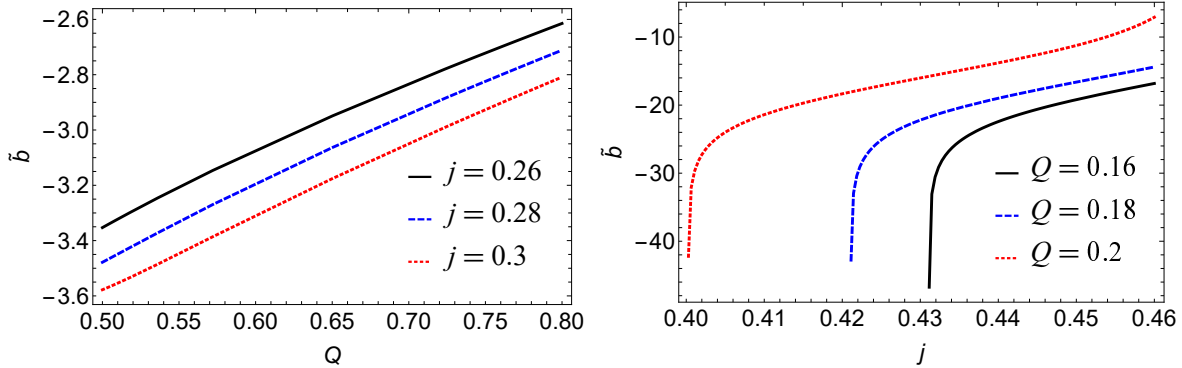


FIG. 16. Plot of the variation of  $\tilde{b}$  with respect to the charge parameter  $Q$  (the left plot) and the rotation parameter  $j$  (the right plot).

the charge parameter. However, the coefficient  $\tilde{b}$  increases with both the charge parameter and the rotation parameter. We also calculated the gravitational time delay effect and showed its variation with the charge parameter and the rotation parameter. In the near future with the advent of new technologies, the detector EHT or square kilometer array may be operated to directly give the photon sphere radius of either the SgrA\* or the M87 supermassive black hole. This may lead to putting constraints on the parameters of the five-dimensional equally rotating black hole in the presence of a cosmological constant. This may help us fix which of the black hole solutions coming from the superstring or supergravity theory may be viable for the experimental extra dimensions to detect.

Gravitational wave astronomy through both the ringdown or electromagnetic observations and the detection of the silhouettes of black holes may provide us hitherto information on the space-time geometry near the black hole event horizon. The ringdown and the silhouettes are directly connected to a particular kind of null circular geodesics called the light rings [81]. For the four-dimensional case, in the asymptotically flat limit for a generic axisymmetric rotating black hole with spherical horizon topology near the event horizon, such light rings (at least one) are formed in each rotation sense [82, 83]. For the five-dimensional case, there exists at least one light ring in the case of both the black hole and the naked singularity [84]. We hope to return to this issue for our concerned black hole in the near future. We also want to explore the timelike circular geodesics in the context of topological configurations for the massive particles as they are important for accumulating particles around the accretion disk.



## ACKNOWLEDGEMENT

This work was supported by the National Natural Science Foundation of China (Grants No. 12347177, No. 11875151 and No. 12247101), the 111 Project under (Grant No. B20063) and Lanzhou City's scientific research funding subsidy to Lanzhou University, the Gansu Province Major Scientific and Technological Special Project.

- 
- [1] B. P. Abbott *et al.* [LIGO Scientific and Virgo], *GW170814: A Three-Detector Observation of Gravitational Waves from a Binary Black Hole Coalescence*, Phys. Rev. Lett. **119**, 141101 (2017).
  - [2] B. P. Abbott *et al.* [LIGO Scientific and Virgo], *Observation of Gravitational Waves from a Binary Black Hole Merger*, Phys. Rev. Lett. **116**, 061102 (2016).
  - [3] B. P. Abbott *et al.* [LIGO Scientific and Virgo], *Tests of General Relativity with GW170817*, Phys. Rev. Lett. **123**, 011102 (2019).
  - [4] B. P. Abbott *et al.* [LIGO Scientific and Virgo], *Tests of General Relativity with the Binary Black Hole Signals from the LIGO-Virgo Catalog GWTC-1*, Phys. Rev. D **100**, 104036 (2019).
  - [5] M. Wielgus, M. Moscibrodzka, J. Vos, Z. Gelles, I. Marti-Vidal, J. Farah, N. Marchili, C. Goddi and H. Messias, *Orbital motion near Sagittarius A\*-Constraints from polarimetric ALMA observations*, Astron. Astrophys. **665**, L6 (2022).
  - [6] R. Abbott *et al.* [KAGRA, VIRGO and LIGO Scientific], *Open Data from the Third Observing Run of LIGO, Virgo, KAGRA, and GEO*, Astrophys. J. Suppl. **267**, 29 (2023).
  - [7] K. Akiyama *et al.*, *First M87 Event Horizon Telescope Results. I. The Shadow of the Supermassive Black Hole*, Astrophys. J. **875**, L1 (2019).
  - [8] K. Akiyama *et al.*, *First M87 Event Horizon Telescope Results. II. Array and Instrumentation*, Astrophys. J. **875**, L2 (2019).
  - [9] K. Akiyama *et al.*, *First M87 Event Horizon Telescope Results. III. Data Processing and Calibration*, Astrophys. J. **875**, L3 (2019).
  - [10] K. Akiyama *et al.*, *First M87 Event Horizon Telescope Results. IV. Imaging the Central Supermassive Black Hole*, Astrophys. J. **875**, L4 (2019).
  - [11] K. Akiyama *et al.*, *First M87 Event Horizon Telescope Results. V. Physical Origin of the Asymmetric Ring*, Astrophys. J. **875**, L5 (2019).
  - [12] K. Akiyama *et al.*, *First M87 Event Horizon Telescope Results. VI. The Shadow and Mass of the Central Black Hole*, Astrophys. J. **875**, L6 (2019).
  - [13] C. Darwin, Proc. R. Soc. A **249**, 180 (1959).
  - [14] S. Frittelli, T. P. Kling and E. T. Newman, *Space-time perspective of Schwarzschild lensing*, Phys. Rev. D **61**, 064021 (2000).

- [15] E. F. Eiroa and C. M. Sendra, *Gravitational lensing by a regular black hole*, *Class. Quant. Grav.* **28**, 085008 (2011).
- [16] V. Bozza, S. Capozziello, G. Iovane and G. Scarpetta, *Strong field limit of black hole gravitational lensing*, *Gen. Rel. Grav.* **33**, 1535 (2001).
- [17] V. Bozza, *Gravitational lensing in the strong field limit*, *Phys. Rev. D* **66**, 103001 (2002).
- [18] V. Bozza and G. Scarpetta, *Strong deflection limit of black hole gravitational lensing with arbitrary source distances*, *Phys. Rev. D* **76**, 083008 (2007).
- [19] V. Bozza, *Quasiequatorial gravitational lensing by spinning black holes in the strong field limit*, *Phys. Rev. D* **67**, 103006 (2003).
- [20] M. Bartelmann and M. Maturi, *Weak gravitational lensing*, [arXiv:1612.06535 [astro-ph.CO]].
- [21] H. Hoekstra and B. Jain, *Weak Gravitational Lensing and its Cosmological Applications*, *Ann. Rev. Nucl. Part. Sci.* **58**, 99 (2008).
- [22] X. M. Kuang and A. Övgün, *Strong gravitational lensing and shadow constraint from M87\* of slowly rotating Kerr-like black hole*, *Annals Phys.* **447**, 169147 (2022).
- [23] I. Sengo, P. Cunha, V.P., C. A. R. Herdeiro and E. Radu, *Kerr black holes with synchronised Proca hair: lensing, shadows and EHT constraints*, *JCAP* **01**, 047 (2023).
- [24] J. P. Luminet, *Image of a spherical black hole with thin accretion disk*, *Astron. Astrophys.* **75**, 228 (1979).
- [25] C. H. Ohanian, *The black hole as a gravitational lensing*, *American Journal of Physics.* **55**, 428 (1987).
- [26] K. S. Virbhadra and G. F. R. Ellis, *Schwarzschild black hole lensing*, *Phys. Rev. D* **62**, 084003 (2000).
- [27] K. S. Virbhadra and G. F. R. Ellis, *Gravitational lensing by naked singularities*, *Phys. Rev. D* **65**, 103004 (2002).
- [28] N. Tsukamoto, *Deflection angle in the strong deflection limit in a general asymptotically flat, static, spherically symmetric spacetime*, *Phys. Rev. D* **95**, 064035 (2017).
- [29] N. Tsukamoto, *Black hole shadow in an asymptotically-flat, stationary, and axisymmetric spacetime: The Kerr-Newman and rotating regular black holes*, *Phys. Rev. D* **97**, 064021 (2018).
- [30] S. U. Islam and S. G. Ghosh, *Strong field gravitational lensing by hairy Kerr black holes*, *Phys. Rev. D* **103**, 124052 (2021).
- [31] S. G. Ghosh, R. Kumar and S. U. Islam, *Parameters estimation and strong gravitational lensing of nonsingular Kerr-Sen black holes*, *JCAP* **03**, 056 (2021).
- [32] R. Whisker, *Strong gravitational lensing by braneworld black holes*, *Phys. Rev. D* **71**, 064004 (2005).
- [33] G. Abbas, A. Mahmood and M. Zubair, *Strong deflection gravitational lensing for photon coupled to Weyl tensor in a charged Kiselev black hole*, *Phys. Dark Univ.* **31**, 100750 (2021).
- [34] E. F. Eiroa, *Gravitational lensing by Einstein-Born-Infeld black holes*, *Phys. Rev. D* **73**, 043002 (2006).
- [35] G. N. Gyulchev and S. S. Yazadjiev, *Kerr-Sen dilaton-axion black hole lensing in the strong deflection limit*, *Phys. Rev. D* **75**, 023006 (2007).

- [36] T. Ghosh and S. Sengupta, *Strong gravitational lensing across dilaton anti-de Sitter black hole*, Phys. Rev. D **81**, 044013 (2010).
- [37] G. N. Gyulchev and I. Z. Stefanov, *Gravitational Lensing by Phantom Black holes*, Phys. Rev. D **87**, 063005 (2013).
- [38] N. U. Molla, A. Ali and U. Debnath, *Observational Signatures of Modified Bardeen Black Hole: Shadow and Strong Gravitational Lensing*, [arXiv:2307.11798 [gr-qc]].
- [39] M. Grespan and M. Biesiada, *Strong Gravitational Lensing of Gravitational Waves: A Review*, Universe **9**, 200 (2023).
- [40] J. Kumar, S. U. Islam and S. G. Ghosh, *Testing Strong Gravitational Lensing Effects of Supermassive Compact Objects with Regular Spacetimes*, Astrophys. J. **938**, 104 (2022).
- [41] R. Kumar Walia, *Observational predictions of LQG motivated polymerized black holes and constraints from Sgr A\* and M87\**, JCAP **03**, 029 (2023).
- [42] J. Kumar, S. U. Islam and S. G. Ghosh, *Investigating strong gravitational lensing effects by supermassive black holes with Horndeski gravity*, Eur. Phys. J. C **82**, 443 (2022).
- [43] X. Lu and Y. Xie, *Gravitational lensing by a quantum deformed Schwarzschild black hole*, Eur. Phys. J. C **81**, 627 (2021).
- [44] M. S. Ali and S. Kauhsal, *Gravitational lensing for stationary axisymmetric black holes in Eddington-inspired Born-Infeld gravity*, Phys. Rev. D **105**, 024062 (2022).
- [45] T. Hsieh, D. S. Lee and C. Y. Lin, *Strong gravitational lensing by Kerr and Kerr-Newman black holes*, Phys. Rev. D **103**, 104063 (2021).
- [46] J. y. Shen, B. Wang and R. K. Su, *The Signals from the brane-world black Hole*, Phys. Rev. D **74**, 044036 (2006).
- [47] C. M. Harris and P. Kanti, *Hawking radiation from a  $(4+n)$ -dimensional rotating black hole*, Phys. Lett. B **633**, 106 (2006).
- [48] M. Casals, P. Kanti and E. Winstanley, *Brane decay of a  $(4+n)$ -dimensional rotating black hole. II. Spin-1 particles*, JHEP **02**, 051 (2006).
- [49] S. Creek, O. Efthimiou, P. Kanti and K. Tamvakis, *Graviton emission in the bulk from a higher-dimensional Schwarzschild black hole*, Phys. Lett. B **635**, 39 (2006).
- [50] P. Kanti and R. A. Konoplya, *Quasi-normal modes of brane-localised standard model fields*, Phys. Rev. D **73**, 044002 (2006).
- [51] P. Kanti, R. A. Konoplya and A. Zhidenko, *Quasi-Normal Modes of Brane-Localised Standard Model Fields. II. Kerr Black Holes*, Phys. Rev. D **74**, 064008 (2006).
- [52] S. Creek, R. Gregory, P. Kanti and B. Mistry, *Braneworld stars and black holes*, Class. Quant. Grav. **23**, 6633 (2006).
- [53] R. A. Konoplya and A. Zhidenko, *Quasinormal modes of black holes: From astrophysics to string theory*, Rev. Mod. Phys. **83**, 793 (2011).

- [54] H. Kodama, R. A. Konoplya and A. Zhidenko, *Gravitational instability of simply rotating AdS black holes in higher dimensions*, Phys. Rev. D **79**, 044003 (2009).
- [55] R. A. Konoplya and A. Zhidenko, *Stability of higher dimensional Reissner-Nordstrom-anti-de Sitter black holes*, Phys. Rev. D **78**, 104017 (2008).
- [56] M. Nozawa and T. Kobayashi, *Quasinormal modes of black holes localized on the Randall-Sundrum 2-brane*, Phys. Rev. D **78**, 064006 (2008).
- [57] S. Chen, B. Wang, R. K. Su and W. Y. P. Hwang, *Greybody factors for rotating black holes on codimension-2 branes*, JHEP **03**, 019 (2008).
- [58] S. Chen, B. Wang and R. K. Su, *Hawking radiation in a rotating Kaluza-Klein black hole with squashed horizons*, Phys. Rev. D **77**, 024039 (2008).
- [59] Y. Liu, S. Chen and J. Jing, *Strong gravitational lensing in a squashed Kaluza-Klein black hole space-time*, Phys. Rev. D **81**, 124017 (2010).
- [60] J. Sadeghi, A. Banijamali and H. Vaez, *Strong Gravitational Lensing in a Charged Squashed Kaluza-Klein Black hole*, Astrophys. Space Sci. **343**, 559 (2013).
- [61] L. Ji, S. Chen and J. Jing, *Strong gravitational lensing in a rotating Kaluza-Klein black hole with squashed horizons*, JHEP **03**, 089 (2014).
- [62] S. Chen, Y. Liu and J. Jing, *Strong gravitational lensing in a squashed Kaluza-Klein Gödel black hole*, Phys. Rev. D **83**, 124019 (2011).
- [63] J. Sadeghi, J. Naji and H. Vaez, *Strong gravitational lensing in a charged squashed Kaluza-Klein Gödel black hole*, Phys. Lett. B **728**, 170 (2014).
- [64] A. S. Majumdar and N. Mukherjee, *Gravitational lensing by higher dimensional black holes*, Contributed to 11th Marcel Grossmann Meeting on General Relativity, 1707.
- [65] S. Chakraborty and S. SenGupta, *Strong gravitational lensing A probe for extra dimensions and Kalb-Ramond field*, JCAP **07**, 045 (2017).
- [66] J. Markeviciute, *Rotating Hairy Black Holes in  $AdS_5 \times S^5$* , JHEP **03**, 110 (2019).
- [67] M. Cvetič, H. Lu and C. N. Pope, *Charged Kerr-de Sitter black holes in five dimensions*, Phys. Lett. B **598**, 273 (2004).
- [68] S. Bhattacharyya, S. Minwalla and K. Papadodimas, *Small Hairy Black Holes in  $AdS_5 \times S^5$* , JHEP **11**, 035 (2011).
- [69] V. P. Frolov and D. Stojkovic, *Particle and light motion in a space-time of a five-dimensional rotating black hole*, Phys. Rev. D **68**, 064011 (2003).
- [70] V. P. Frolov and D. Stojkovic, *Quantum radiation from a five-dimensional rotating black hole*, Phys. Rev. D **67**, 084004 (2003).
- [71] J. Markeviciute and J. E. Santos, *Evidence for the existence of a novel class of supersymmetric black holes with  $AdS_5 \times S^5$  asymptotics*, Class. Quant. Grav. **36**, 02LT01 (2019).
- [72] S. Tomizawa and T. Igata, *Stable circular orbits in Kaluza-Klein black hole spacetimes*, Phys. Rev. D **103**, 124004 (2021).

- [73] J. Kormendy and L. C. Ho, *Coevolution (Or Not) of Supermassive Black Holes and Host Galaxies*, Ann. Rev. Astron. Astrophys. **51**, 511 (2013).
- [74] R. Gavazzi, T. Treu, L. V. E. Koopmans, A. S. Bolton, L. A. Moustakas, S. Burles, P. J. Marshall, Astrophys. J., **677**, 1046 (2008).
- [75] T. Do et al., *Unprecedented variability of Sgr A\* in NIR*, Science **365**, 664 (2019).
- [76] V. Bozza and L. Mancini, *Time delay in black hole gravitational lensing as a distance estimator*, Gen. Rel. Grav. **36**, 435 (2004).
- [77] T. Hsieh, D. S. Lee and C. Y. Lin, *Gravitational time delay effects by Kerr and Kerr-Newman black holes in strong field limits*, Phys. Rev. D **104**, 104013 (2021).
- [78] X. Lu, F. W. Yang and Y. Xie, *Strong gravitational field time delay for photons coupled to Weyl tensor in a Schwarzschild black hole*, Eur. Phys. J. C **76**, 357 (2016).
- [79] S. Sahu, M. Patil, D. Narasimha and P. S. Joshi, *Can strong gravitational lensing distinguish naked singularities from black holes?*, Phys. Rev. D **86**, 063010 (2012).
- [80] N. Tsukamoto, T. Harada and K. Yajima, *Can we distinguish between black holes and wormholes by their Einstein ring systems?*, Phys. Rev. D **86**, 104062 (2012).
- [81] V. Cardoso, E. Franzin and P. Pani, *Is the gravitational-wave ringdown a probe of the event horizon?*, Phys. Rev. Lett. **116** (2016), 171101, Erratum: Phys. Rev. Lett. **117**, 089902 (2016).
- [82] P. V. P. Cunha and C. A. R. Herdeiro, *Stationary black holes and light rings*, Phys. Rev. Lett. **124**, 181101 (2020).
- [83] S. P. Wu and S. W. Wei, *Topology of light rings for extremal and non-extremal Kerr-Newman Taub-NUT black holes without  $\mathbb{Z}_2$  symmetry*, [arXiv:2307.14003 [gr-qc]].
- [84] A. Tavlayan and B. Tekin, *Light rings around five-dimensional stationary black holes and naked singularities*, Phys. Rev. D **107**, 024016 (2023).